

Spectro-photometric distances to stars: a general-purpose Bayesian approach

Basílio X. Santiago^{1,2}, Dorothée E. Brauer³, Friedrich Anders³, Cristina Chiappini^{3,2}, Léo Girardi^{4,2}, Helio J. Rocha-Pinto^{5,2}, Eduardo Balbinot^{1,2}, Luiz N. da Costa^{6,2}, Marcio A.G. Maia^{6,2}, Mathias Schultheis⁷, Matthias Steinmetz³, Andrea Miglio⁸, Josefina Montalbán⁹, Donald P. Schneider^{10,11}, Timothy C. Beers¹², Peter M. Frinchaboy¹³, Young Sun Lee¹⁴, and Gail Zasowski¹⁵

¹ Instituto de Física, UFRGS, Caixa Postal 15051, Porto Alegre, RS - 91501-970, Brazil

² Laboratório Interinstitucional de e-Astronomia - LIneA, Rua Gal. José Cristino 77, Rio de Janeiro, RJ - 20921-400, Brazil

³ Leibniz-Institut für Astrophysik Potsdam (AIP), An der Sternwarte 16, 14482, Potsdam, Germany.

⁴ Osservatorio Astronomico di Padova - INAF, Vicolo dell'Osservatorio 5, I - 35122 Padova, Italy

⁵ Universidade Federal do Rio de Janeiro, Observatório do Valongo, Ladeira do Pedro Antônio 43, 20080-090 Rio de Janeiro, Brazil

⁶ Observatório Nacional, Rua Gal. José Cristino 77, Rio de Janeiro, RJ - 20921-400, Brazil

⁷ Observatoire de la Cote d'Azur, Laboratoire Lagrange, CNRS UMR 7923, B.P. 4229, 06304 Nice Cedex, France

⁸ School of Physics and Astronomy, University of Birmingham, Edgbaston, Birmingham, B15 2TT, United Kingdom

⁹ Institut d'Astrophysique et de Géophysique, Allée du 6 août, 17 - Bât. B5c, B-4000 Liège 1 (Sart-Tilman), Belgium

¹⁰ Department of Astronomy and Astrophysics, The Pennsylvania State University, University Park, PA 16802

¹¹ Institute for Gravitation and the Cosmos, The Pennsylvania State University, University Park, PA 16802

¹² National Optical Astronomy Observatory and JINA: Joint Institute for Nuclear Astrophysics, Tucson, AZ 85719 USA

¹³ Department of Physics & Astronomy, Texas Christian University, TCU Box 298840, Fort Worth, TX 76129

¹⁴ Department of Astronomy, New Mexico State University, Las Cruces, NM, 88003, USA

¹⁵ Dept of Physics and Astronomy, Johns Hopkins University, Baltimore, MD, 21210, USA

June 16, 2022

ABSTRACT

Context. Determining distances to individual stars is a necessary step towards mapping Galactic structure and determining spatial variations in the chemo-dynamical properties of stellar populations in the Milky Way.

Aims. We have developed a procedure that estimates distances to stars using measured spectroscopic and photometric quantities. Similar to other recent works in the literature, it employs a Bayesian approach to build the probability distribution function over stellar evolutionary models given the data, delivering estimates of expected values of model parameters (including distances) for each star individually. Our method provides several alternative distance estimates for each star in the output, along with their associated uncertainties.

Methods. The code was first tested on simulations, successfully recovering input distances to mock stars with errors that scale with the uncertainties in the adopted spectro-photometric parameters, as expected. The code was then validated by comparing our distance estimates to parallax measurements from the Hipparcos mission (ESA 1997) for nearby stars (< 60 pc), to asteroseismic distances of CoRoT red giant stars, and to known distances of well-studied open and globular clusters. The photometric data of these reference samples cover both the optical and near infra-red wavelengths. The spectroscopic parameters are also based on spectra taken at various wavelengths, with varying spectral coverage and resolution: the Radial Velocity Experiment, the Sloan Digital Sky Survey programs SEGUE and APOGEE, and the ESO HARPS instrument.

Results. For Hipparcos and CoRoT samples, the typical random distance scatter is $\approx 20\%$ or less, both for the nearby and farther data. There is a trend towards underestimating the distances by < 10%. The comparison to star clusters from SEGUE and APOGEE has led to systematic differences < 5% for most cluster stars although with significant scatter. Finally, we tested our distances against those previously determined for a high quality sample of giant stars from the RAVE survey, again finding a reasonable agreement, with only a small systematic trend. Efforts are underway to provide our code to the community by running it on a public server.

Key words. Stellar populations; Galaxy evolution; stellar statistics

1. Introduction

A crucial step towards studying the stellar populations and their variation across the Galaxy is to measure reliable stellar distances. The parallax method is currently viable for only a small fraction of local stars, although the recently launched Gaia satellite (Perryman et al. 2001) is expected to dramatically increase the number of parallax and proper motion measurements. Precise distances may also be obtained from asteroseismology, but only for a fraction of stars subject to systematic variability studies (Miglio et al. 2013b; Rodrigues et al. 2014). Indirect methods of distance determination, based on photometric and spectroscopic quantities and their relation to stellar absolute magnitudes, can be used for much more distant stars. Photometric distances have been applied to multi-band optical and near infrared data from different surveys to model the spatial distribution of Galactic stars and to study its substructures (e.g., Jurić et al. 2008; Correnti et al. 2010; Minniti et al. 2011). Recent Sloan Digital Sky Survey III (SDSS-III, Eisenstein et al. 2011) spectroscopic surveys, such as the Sloan Extension for Galactic Understanding and Exploration (SEGUE, Yanny et al. 2009) and the Apache Point Observatory Galactic Evolution Experiment (APOGEE, Allende Prieto et al. 2008a) have produced many more observational constraints, including stellar atmospheric parameters, kinematical and chemical data, that can be used to estimate reliable distances to tens of thousands of stars sampled from the SDSS and 2MASS (Skrutskie et al. 2006) photometric data. These surveys have already had a clear impact on our understanding of the Galaxy (Carollo et al. 2010; Lee et al. 2011b; Schlesinger et al. 2012; Carollo et al. 2012; Cheng et al. 2012; Bovy et al. 2012a,b; Hayden et al. 2014; Anders et al. 2014). The recently completed RAdial Velocity Experiment (RAVE) survey (Steinmetz et al. 2006) has also provided atmospheric parameters, radial velocities and chemical abundances for six individual elements for more than 400 000 stars (Kordopatis et al. 2013).

Future spectroscopic surveys, such as those planned as part of the Sloan Digital Sky Survey IV (SDSS-IV¹), the Galactic Archaeology with HERMES (GALAH²), the LAMOST Experiment for Galactic Understanding and Exploration (LEGUE, Deng et al. 2012) and the now ongoing Gaia ESO Survey (GES - Gilmore et al. 2012), will continuously increase the number of stars with available spectroscopic information. In fact, these large spectro-photometric data sets already available or in the making will, when analyzed together, allow a description of the structure and substructures of the Galaxy with unprecedented detail, excellent statistics, and full use of the 6D phase-space information. Phase-space reconstruction of the stellar distribution, coupled to spectroscopic abundances for large samples, will continue to provide challenging quantitative tests to models of Galaxy formation and evolution.

In order to take full advantage of the large set of available spectroscopic and photometric parameters from recent surveys, probabilistic inference has been used by several authors to infer ages, absolute magnitudes, extinction, distances, among other parameters (e.g., Pont & Eyer 2004; Jørgensen & Lindgren 2005; Bailer-Jones 2011; Serenelli et al. 2013; Schönrich & Bergemann 2014). In the context of stellar distances, a series of papers with increasing levels of sophistication has been presented by the RAVE collaboration (Breddels et al. 2010; Zwitter et al. 2010; Burnett & Binney 2010). Burnett & Binney (2010) make use of a comprehensive set of measured parameters and

their estimated uncertainties to infer, for each star, the probability distribution that a set of chosen stellar models generate the data. The method was further refined and used to study Galactic chemistry by Burnett et al. (2011) and Binney et al. (2014).

In this paper, we follow a similar theoretical background as those authors and implement a code that computes spectro-photometric distances with the goal of mapping large stellar samples in three dimensions or in phase-space. We are motivated by the analyses of SDSS-III SEGUE and APOGEE data being led by the Brazilian Participation Group (BPG) and the Leibniz-Institut für Astrophysik Potsdam (AIP), which are presented in Anders et al. (2014) and *Brauer et al. 2015 (in prep.)*. These papers use APOGEE giants and SEGUE G-dwarfs, respectively, to improve chemo-dynamical constraints to the Galactic components, especially the discs. Since SEGUE and APOGEE targets were selected based on different photometric data and have different spectral coverage and resolution, our basic challenge is to ensure that reasonably accurate distances are computed for datasets of vastly different provenance. Our emphasis is therefore on confronting our distance estimates with as many reference samples as possible. A direct comparison with the RAVE distances obtained by Binney et al. (2014) for the high-quality giant sample studied in Boeche et al. (2013) is also provided. In Table 1 we list the main characteristic of the surveys we have applied our method to.

The outline of the paper is as follows. In §2 we review the method, introduce our notation, and show the results of initial validation tests. We discuss prior assumptions and selection effects that may influence the estimated distances. An analysis of the different uncertainty estimates and their comparison is also provided. In §3 we compare our distances to several previous distance determinations that can be used as a reference, given their higher precision and more controlled systematics. Our summary and conclusions are provided in §4.

2. The method

The general method adopted for this study uses a set of measured photometric and spectroscopic parameters, such as metallicity $[Fe/H]$, alpha element enhancement $[\alpha/Fe]$, effective temperature T_{eff} , surface gravity $\log g$, intrinsic apparent magnitude m , and colors, to estimate the distance to individual stars. These quantities are compared to predictions from stellar evolutionary models. The comparison between model and measured parameters follows a statistical approach that is similar to previous works (Burnett & Binney 2010; Burnett et al. 2011; Binney et al. 2014).

In brief, assuming that the errors in the measured parameters follow a normal distribution, the probability that a measured value of some quantity $x \pm \sigma_x$ is consistent with some theoretical value x_0 is given by

$$P(x, \sigma_x | x_0) = \frac{1}{\sigma_x \sqrt{2\pi}} \exp[-(x - x_0)^2 / 2\sigma_x^2]. \quad (1)$$

We can extend this reasoning to a set of parameters $\mathbf{x} \pm \sigma_{\mathbf{x}}$, whose theoretical values according to a stellar model are \mathbf{x}_0 , by writing:

$$P(\mathbf{x}, \sigma_{\mathbf{x}} | \mathbf{x}_0) = \prod_i \frac{1}{\sigma_{x,i} \sqrt{2\pi}} \exp[-(x_i - x_{0,i})^2 / 2\sigma_{x,i}^2], \quad (2)$$

where the product is taken over all the measured parameters of a single star being confronted to the model values. The expression

¹ <http://www.sdss3.org/future/>

² <http://www.mso.anu.edu.au/galah/home.html>

Table 1. Surveys for which distances were computed using the method presented in this paper.

Survey	Year	N_{stars}	Spatial coverage (sq. deg.)	Typical S/N	λ range	R
SEGUE-1 (G dwarfs)	2004-2008	$\approx 120,000$ (35000)	$\approx 1,300$	25	$0.38 - 0.92\mu\text{m}$	2,000
APOGEE (DR10 HQ giants)	2011-2014	$\approx 100,000$ (22000)	$\approx 2,800$	100	$1.5 - 1.7\mu\text{m}$	22,500
RAVE (HQ giants)	2006-2013	$\approx 500,000$ (9000)	$\approx 20,000$	30	$0.84 - 0.88\mu\text{m}$	7,500

above gives the probability of measuring the set $\mathbf{x} \pm \sigma_{\mathbf{x}}$ given a model. This equals the likelihood function over the models. The joint probability that the data set $\mathbf{x} \pm \sigma_{\mathbf{x}}$ and model \mathbf{x}_0 occur is given by the conditional probability of Equation (2) multiplied by the model probability itself, $P(\mathbf{x}_0)$, as

$$P(\mathbf{x}, \sigma_{\mathbf{x}}, \mathbf{x}_0) = P(\mathbf{x}, \sigma_{\mathbf{x}} | \mathbf{x}_0) P(\mathbf{x}_0).$$

The model probability function $P(\mathbf{x}_0)$ will be described in detail below. According to Bayes' theorem, we may compute the posterior probability distribution as:

$$P(\mathbf{x}_0 | \mathbf{x}, \sigma_{\mathbf{x}}) = \frac{P(\mathbf{x}, \sigma_{\mathbf{x}} | \mathbf{x}_0) P(\mathbf{x}_0)}{P(\mathbf{x}, \sigma_{\mathbf{x}})}, \quad (3)$$

where the denominator is the model evidence and depends only on the measured parameters and their uncertainties.

Therefore, in order to evaluate some specific model quantity θ (which may or may not belong to the set \mathbf{x}_0) for a given star, we take the first moment of the distribution given by Equation (3):

$$\bar{\theta} = \int \theta P(\mathbf{x}_0 | \mathbf{x}, \sigma_{\mathbf{x}}) d\theta. \quad (4)$$

As mentioned earlier, a typical set of measured parameters includes $\mathbf{x} = \{[M/H], T_{\text{eff}}, \log g, \text{colors}, m\}$. As for the stellar models, besides the theoretical values of the same parameters, they also involve other quantities such as mass m_{\star} , age τ , and absolute magnitude M_{abs} . And we take $\theta = s$, where s is the star's model distance computed as $s [\text{pc}] = 10^{0.2(m - M_{\text{abs}} + 5)}$.

Initial tests showed that $\log g$ is critical to estimate unbiased distances, since it is the quantity that best discriminates between low-luminosity dwarfs and more luminous giants, which otherwise share similar values of temperature, abundances and colors. Dropping $\log g$ from the fitting procedure leads to overestimated distances for dwarf stars, and underestimated distances to giants, respectively. Similar tests also showed that cutting models with $|\mathbf{x}_0 - \mathbf{x}| > 3\sigma_{\mathbf{x}}$ decreases the processing time without appreciably changing the final distance estimates.

Based on these initial assessments, we implemented a code that estimates distances using the method described above and based on four distinct sets \mathbf{x} :

1. $\mathbf{x} = \{[M/H], T_{\text{eff}}, \log g, m, \text{colors}\}$
2. $\mathbf{x} = \{[M/H], T_{\text{eff}}, \log g, m\}$
3. $\mathbf{x} = \{[M/H], \log g, m, \text{colors}\}$
4. $\mathbf{x} = \{[M/H], m, \text{colors}\}$, but with a cut in models whose $\log g$ differs by more than 0.5 dex from the measured value.

The code can accommodate other sets if so desired. The advantage of implementing different sets of parameters for distance determination is to provide flexibility: distances can be estimated even in the absence of one or two parameters from the set with the largest number of parameters (set 1). Furthermore, the alternative distance estimates may be intercompared to provide a means to evaluate the sensitivity of the method to the particular combination of spectroscopic and photometric parameters adopted (see §2.2).

Often, the data set in a given sample includes only $[\text{Fe}/\text{H}]$ values, which are used in place of $[M/H]$. When $[\alpha/\text{Fe}]$ values are available, we adopt the empirical relation $[M/H] = [\text{Fe}/\text{H}] + [\alpha/\text{Fe}]$. Another important issue is extinction: the photometric data, m and colors, must be corrected for extinction and reddening in order to be compared to the models. The exact procedure depends on the bandpasses used, on the available extinction estimates and on the assumed extinction coefficients.

Fig. 1 shows the results of applying the method to a simulated set of stars. The figure shows the distribution of the relative distance errors, $(s_{\text{BPG}} - s_{\text{TRUE}})/s_{\text{TRUE}}$ (where *BPG* refers to the distances computed in this work), for the four parameter sets listed above. The models used to create fake stars were those from the Padova TRIeste Stellar Evolution Code (PARSEC, Bressan et al. 2012), with a narrow metallicity step of $[M/H] = 0.1$ spanning the range $-2.2 \leq [M/H] \leq 0.6$, and age steps of $\log \tau(\text{yrs}) = 0.05$ in the range $6.0 \leq \log \tau(\text{yrs}) \leq 10.2$. Stars were randomly picked from the model isochrones and assigned a fixed intrinsic distance modulus of $(m - M)_0 = 12.5$, which corresponds to a distance of $s = 3.16$ kpc. Random Gaussian errors were added to the set of model quantities $\mathbf{x}_0 = \{[M/H], T_{\text{eff}}, \log g, m, \text{colors}\}$, generating a set of corresponding measurements \mathbf{x} . The simulated photometry was in the near infra-red (JHK), with no extinction applied. For the results shown in the figure we adopted $\sigma_{T_{\text{eff}}} = 100\text{K}$, $\sigma_{[M/H]} = 0.05$, $\sigma_{\log g} = 0.1$, and $\sigma_{\text{mag}} = 0.02$. The relative distance residuals are shown in Fig. 2 as a function of three main parameters.

The four distance estimates that we propose lead to reasonable results as attested by the error distributions. There is a systematic degradation in the distances as we move down from set 1 to 4. Set 1, for instance, yields mean distance errors of $< 1\%$ with a rms of 18%. For the other three sets, these numbers are $2.0\% \pm 22\%$, $3.6\% \pm 23\%$, $8.2\% \pm 28\%$, respectively. This is expected, at least in the context of simulations, since usage of more measured parameters will tend to constrain the stellar models that best describe each star.

Figure 2 shows that the distance errors are not correlated with the parameters themselves. We tested the effect of increasing the uncertainties in the three main parameters. When broader Gaussian errors, with $\sigma_{T_{\text{eff}}} = 300\text{K}$, $\sigma_{[M/H]} = 0.2$, $\sigma_{\log g} = 0.25$, and $\sigma_{\text{mag}} = 0.10$ are used, the mean and rms distance errors for set 1 increase to 13% and 44% respectively, attesting the strong dependence of method's precision on the parameter measurement uncertainties. The simulations were also carried out using a larger value of $s_{\text{TRUE}} = 7.9$ kpc, with nearly identical results.

2.1. The model priors

We use our current knowledge about the Galactic and its components to build the model prior probability distribution, $P(\mathbf{x}_0)$, including basic information concerning the distributions of stars as a function of position, mass, age, and metallicity. We assume that all stars follow a Chabrier initial mass function (IMF, Chabrier 2003) and incorporate the probability that a randomly selected star falls within a given mass range, $p(\text{mass})$. This involves an

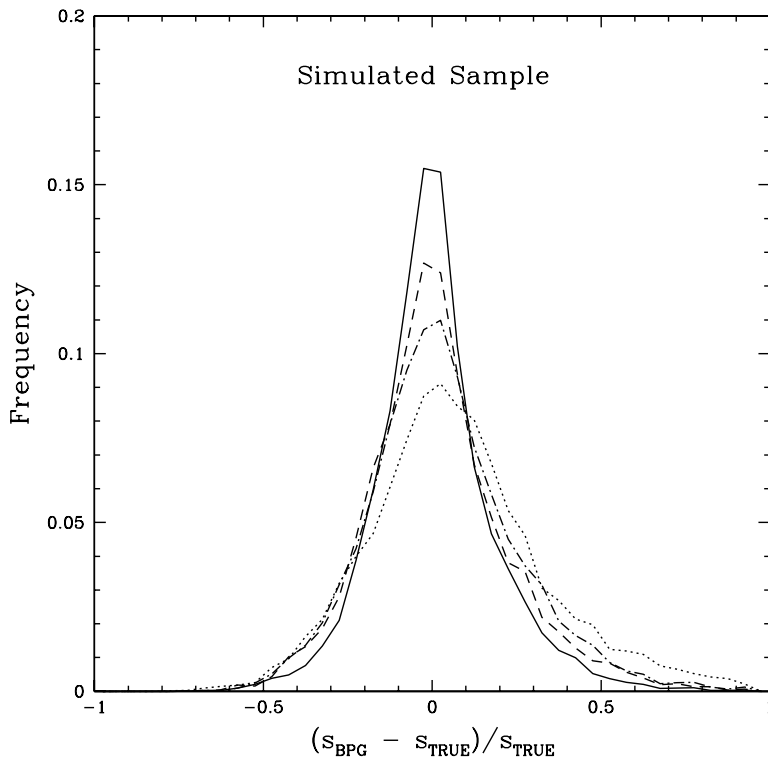


Fig. 1. Distribution of relative distance errors, $(s_{\text{BPG}} - s_{\text{TRUE}})/s_{\text{TRUE}}$, for a sample of simulated stars taken from PARSEC models (see text), and using the distances based on the four sets of measured parameters listed in §2: set (1) ($\mathbf{x} = \{[M/H], T_{\text{eff}}, \log g, m, \text{colors}\}$): solid line; set (2) ($\mathbf{x} = \{[M/H], T_{\text{eff}}, \log g, m\}$): dashed line; set (3) ($\mathbf{x} = \{[M/H], \log g, m, \text{colors}\}$): dot-dashed line; set (4) ($\mathbf{x} = \{[M/H], m, \text{colors}\}$, but cut at $\Delta \log g < 0.5 \text{ dex}$): dotted line.

integral over the mass function which is provided in the model isochrones.

We assume different age and spatial distributions for the basic Galactic components, namely the thin disc, the thick disc, and the spheroid. The age distributions, $p(\text{age})$, are taken to be uniform with an upper limit of 10 Gyrs for the thin disc, and lower limits of 8 and 10 Gyrs for the thick disc and halo, respectively.

The spatial priors for the thin and thick disks are given, respectively, by

$$p_{\text{thin}}(R, z) \propto s^2 ds \cdot \exp(-R/h_{R,\text{thin}}) \cdot \exp(-|z|/h_{z,\text{thin}})$$

$$p_{\text{thick}}(R, z) \propto s^2 ds \cdot \exp(-R/h_{R,\text{thick}}) \cdot \exp(-|z|/h_{z,\text{thick}}),$$

where (R, z) are cylindrical coordinates with origin at the Galactic center, whose values are computed given a model distance

s and a direction (l, b) , and h_R and h_z are the respective scale lengths and heights; We adopt the same Galactic structural parameters as Burnett et al. (2011). In computing the cylindrical coordinates, we use $R_0 = 8.5$ kpc as the distance from the Sun to the Galactic centre.

For the halo, we assume a power-law density profile with spherical symmetry:

$$p_{\text{halo}}(r, l, b) \propto r^{-\gamma} \cdot s^2 ds,$$

where $r(s, l, b)$ is a radial spherical coordinate. Again, as in Burnett et al. (2011), we adopt $\gamma = 3.39$.

The three density profiles are normalized at the solar location, which, for simplicity, we take to be $(R, z) = (R_0, 0)$ and $r = R_0$, respectively, in cylindrical and spherical coordinates. The normalization values are again taken from Burnett et al. (2011).

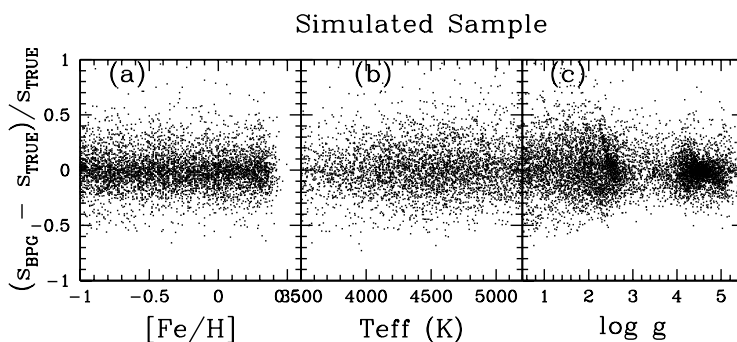


Fig. 2. Relative distance errors of the simulated stars shown as a function of the main model parameters. A $s_{\text{TRUE}} = 3.16$ kpc was attributed to all synthetic stars. The panels show the relative residuals in the estimated distances plotted against $[M/H]$ (panel (a)), T_{eff} (panel (b)), and $\log g$ (panel (c)) for Gaussian errors with $\sigma_{T_{\text{eff}}} = 100\text{K}$, $\sigma_{[M/H]} = 0.05$, $\sigma_{\log g} = 0.1$, and $\sigma_{\text{mag}} = 0.02$.

We assume that the three basic Galactic components follow Gaussian metallicity distribution functions (MDFs), $p_i([M/H])$, exactly as described by Burnett et al. (2011). Our final model prior is then given as

$$P(\mathbf{x}_0) = p(\text{mass}) \sum_i p_i(\text{age}) p_i(\mathbf{r}) p_i([M/H])$$

In Fig. 3, we assess the effect of the adopted model priors on the distance estimates. The top row panels compare distances based on all priors to those using only the spatial ones. The distances in the lower panels include the age priors, but still exclude the MDFs. We use the high quality sample from RAVE ($\approx 9,000$ stars; see §3.4) in the figure. We restrict our comparison to the distance estimates from parameter sets (1) and (2) listed in §2 (left and right panels of Fig. 3, respectively). It is clear from the figure that inclusion of age and metallicity priors both tend to systematically reduce the distances of a significant

fraction of the stars. Restricting the thick disc and halo samples to old ages, in particular, prevents models of young luminous stars to be included in their distance estimates. Similarly, associating disc stars to relatively metal-rich models also tends to reduce their distances. A large number of stars are unaffected by the specific choice of model priors. Using all stars with estimated distances $s < 6$ kpc (when all priors are included, comprising the vast majority of the RAVE high quality sample) we obtain a mean residual of 5% and a scatter of 6% between the *all priors* and *spatial priors only* distances. This is, in fact, smaller than the systematic residuals and scatter found with respect to more precisely determined distances, as will be discussed in §3.

2.2. Distance Uncertainties

Following Burnett et al. (2011), we compute the square root of the second-order moment of the distance s over the posterior

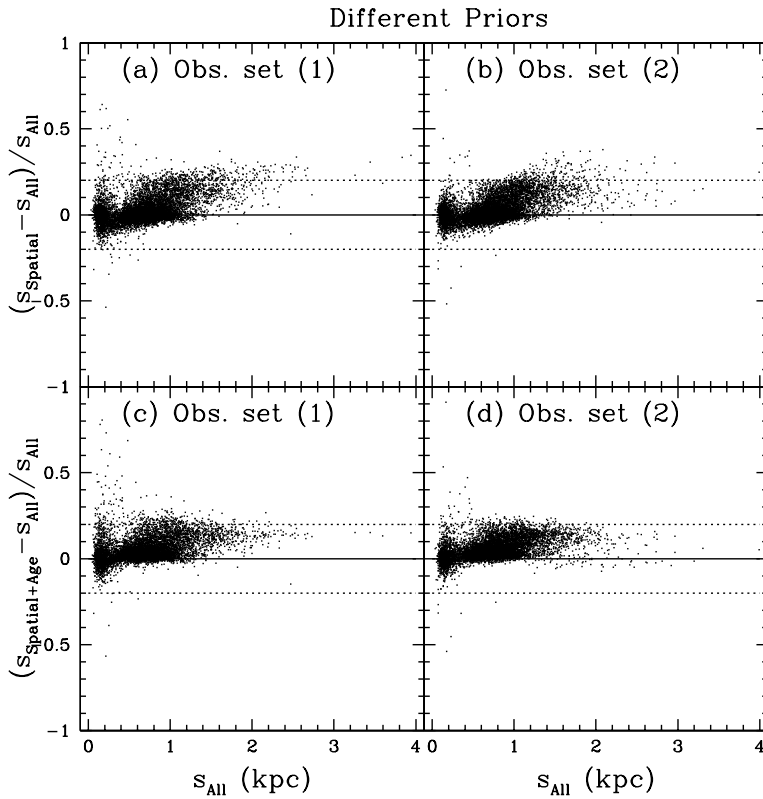


Fig. 3. Comparison of our spectro-photometric distances (BPG) for $\approx 9,000$ giant stars from RAVE (see §3.4) as computed under different model priors. Panel (a): Relative difference in the distances using only spatial priors plotted against distances using all priors mentioned in §2.1. Distances are computed using the data set (1) listed in §2 ($\mathbf{x} = \{[M/H], T_{\text{eff}}, \log g, m, \text{colors}\}$). Panel (b): Same as in panel (a), but now using the data set (2) listed in §2 ($\mathbf{x} = \{[M/H], T_{\text{eff}}, \log g, m\}$). Panel (c): Same as in panel (a), but now adding age priors to the spatial ones. Panel (d): Same as in panel (c), but now using the data set (2) listed in §2 ($\mathbf{x} = \{[M/H], T_{\text{eff}}, \log g, m\}$).

probability distribution $P(\mathbf{x}_0|\mathbf{x}, \sigma_{\mathbf{x}})$ (after subtraction of the estimated distance squared) in order to determine the uncertainty in the distance of each star.

In addition, we estimate distance uncertainties in two other ways. First, we calculate the difference between the weighted average value given by Equation (4) and the value that corresponds to the peak in the model probability distribution given by Equation (3). This *internal uncertainty* is a simple way to quantify how complex the model pdf is for each star, since it should be small for a single peaked, symmetric model pdf. Secondly, we evaluate the maximum difference among the four distance estimates listed earlier. This is an *external uncertainty* that quantifies the sensitivity of the distance estimates to the set of measured parameters used.

The panels in Fig. 4 show the distributions of relative uncertainties, σ_s/s , for the four different choices of \mathbf{x} listed in §2. In

each panel, the three estimates are presented. The *external uncertainty* (dashed line) is the same in all panels and should serve as a comparison guide. The stars used in the figure are from a large sample of G-dwarfs from the SEGUE survey, which is studied by *Brauer et al. 2015 (in prep.)* (see §3.3).

The panels appear very similar except for panel (b), which shows the results when colors are not used in the data set to be compared to the models. For this particular case, both the *internal* and *rms* uncertainties tend to be larger. This increase may result from the comparatively larger uncertainties in the spectroscopic parameters, especially $\log g$, with respect to the photometric ones. It is clear from the figure that in most cases the width of the model pdf, quantified by its rms value, is the dominant source of uncertainty.

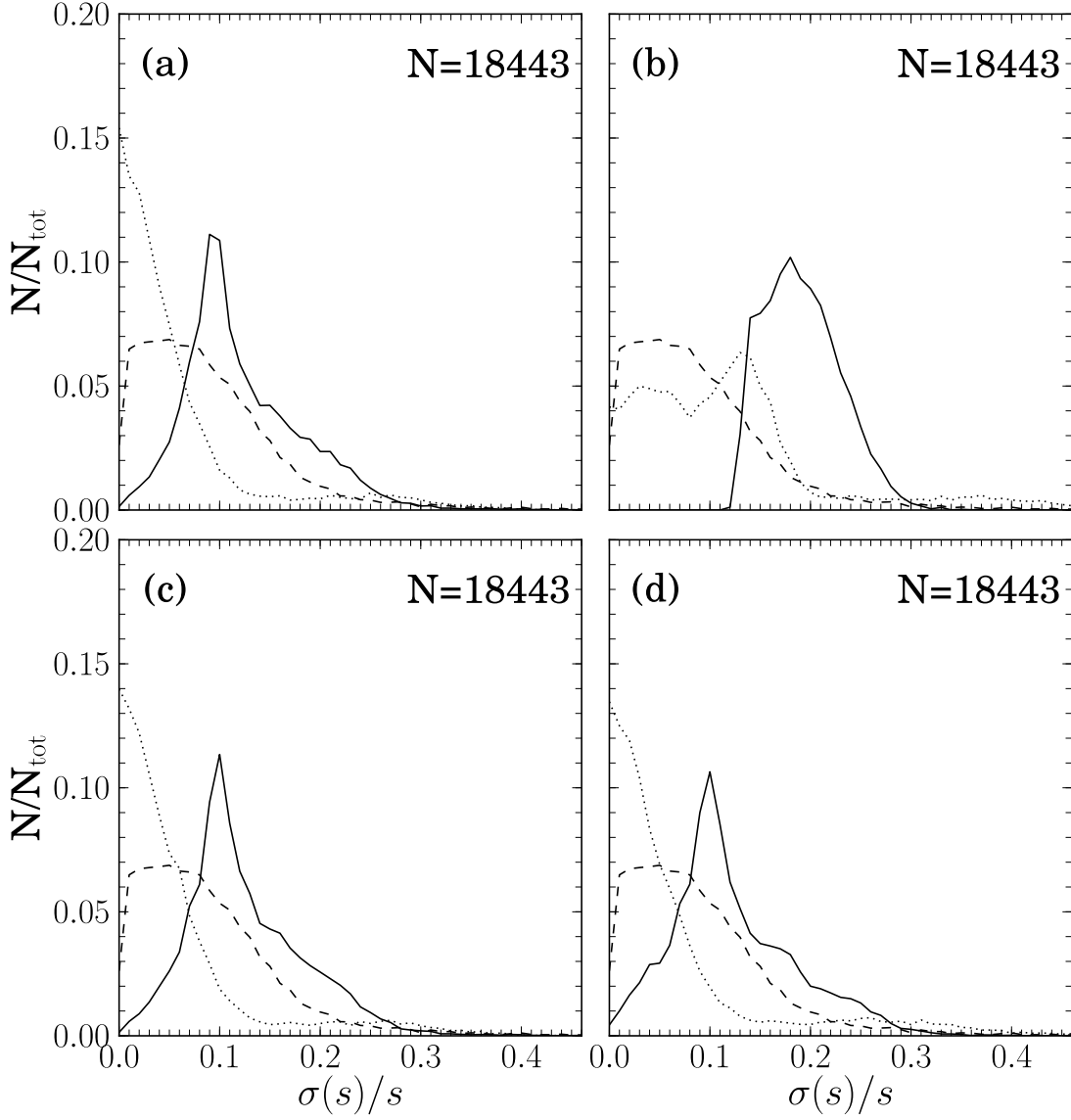


Fig. 4. Panel (a): Distribution of uncertainties for the distances computed with the parameter set (1) ($\mathbf{x} = \{[M/H], T_{\text{eff}}, \log g, m, \text{colors}\}$). The solid line corresponds to the uncertainty based on the rms value of the model pdf. The dotted line is the *internal error*, as defined in the text. The dashed line is the *external error*, as defined in the text. Panel (b): Same as in panel (a), but now showing the distribution of uncertainties for the distances computed with the parameter set (2) ($\mathbf{x} = \{[M/H], T_{\text{eff}}, \log g, m\}$). Panel (c): Same as in panel (a), but now showing the distribution of uncertainties for the distances computed with the parameter set (3) ($\mathbf{x} = \{[M/H], \log g, m, \text{colors}\}$). Panel (d): Same as in panel (a) but now showing the distribution of uncertainties for the distances computed with the parameter set (4) ($\mathbf{x} = \{[M/H], m, \text{colors}\}$) but with models cut at $\Delta \log g > 0.5$.

3. Method Validation

In this section, we present results of the application of our method described in the previous section to a number of reference samples for distance determination. As in the previous sections, we use s_{BPG} to refer to our distances in all figures. Those taken as reference are referred to as s_{REF} . In Table 2, we provide information about the source, derivation methods and precision of the parameters in the reference samples. The results of the comparison with the reference samples are summarized in Table 3. We also compare our distance estimates with those obtained by Binney et al. (2014) for a sample of stars from RAVE. This last comparison represents a cross-check of the implementation of the algorithm, as the authors follow similar theoretical background.

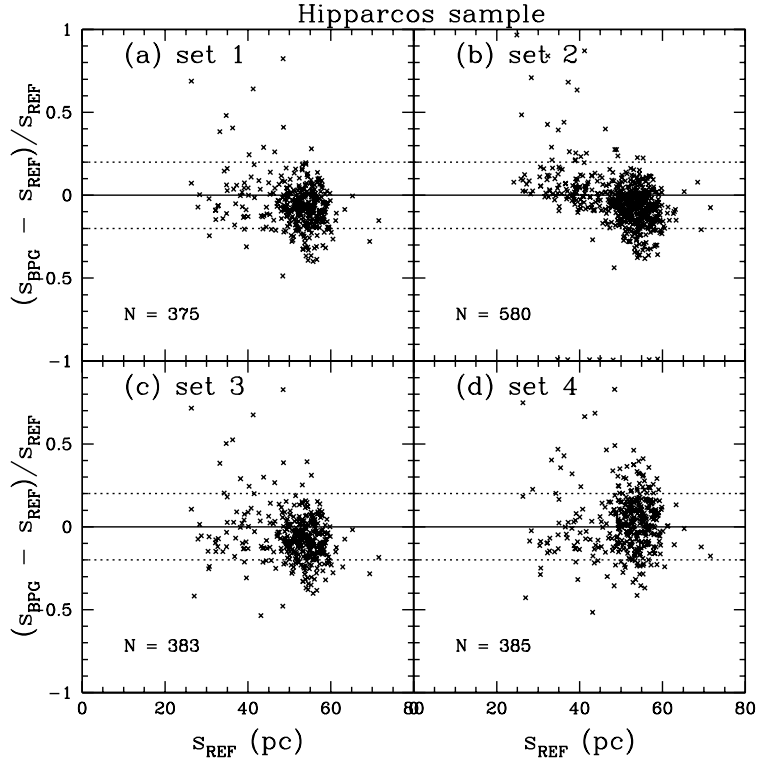


Fig. 5. Comparison of our spectro-photometric distances with distances based on high-precision trigonometric parallaxes obtained by the Hipparcos satellite. In all panels we show the relative distance residuals. Panel (a): Spectro-photometric distances based on the parameter set (1) listed in §2 plotted against Hipparcos distances. The number of stars plotted is shown in the panel. The central solid line is the identity line, whereas the upper and lower ones indicate deviations at the 20% level; Panel (b): Same as in panel (a), but now using distances estimated with set (2) as listed in §2; Panel (c): Same as in previous panels, but now using distances estimated with set (3) listed in §2; Panel (d): Same as in previous panels, but now using distances estimated with set (4) listed in §2.

Table 2. Summary of the reference data: provenance, parameter range and uncertainties. $\log g$ values in the APOGEE/CoRoT sample are based on asteroseismology measurements. APOGEE cluster sample had ASPCAP $\log g$ recalibrated using stars in common with CoRoT. All other non-photometric parameters were derived spectroscopically.

Sample	d source	d range (kpc)	T_{eff} source	δT_{eff} (K)	range (K)	$\log g$ source	$\delta \log g$	range	[Fe/H] source	δ [Fe/H]	range	photom.
Hipparcos-HARPS	van Leeuwen 2007	<0.06	Sousa 2011	80	4400-6800	Sousa 2011	0.1	3.5-4.8	Sousa 2011	0.1	-1.0-0.5	BVI
APOGEE CoRoT	Miglio 2013a	1-6	Ahn 2014	150	4100-5100	Miglio 2013a	0.05	Ahn 2014	1.6-3.0	0.1	-0.8-0.5	JHK_s
APOGEE Clusters	WEBDA,Harris et al	1-6	Anders 2014	150	3700-5000	Pinsonneault 2014	0.2	1.0-3.4	Meszáros 2013	0.1	-1.0-0.5	JHK_s
SEGUE Clusters	WEBDA,Harris et al	1-12	Ahn 2012	130	4700-7000	Ahn 2012	0.21	1.6-5.0	Ahn 2012	0.11	-3.0-0.0	ugriz

3.1. Comparison with the Hipparcos scale - The HARPS FGK sample

As a first validation test of our spectro-photometric distance algorithm, we use the high-resolution HARPS FGK dwarf sample of 582 nearby stars with well-determined atmospheric parameters by Sousa et al. (2011). Hereafter, we will refer to this sample as the *Hipparcos sample*, because for these stars precision parallaxes from Hipparcos (Perryman et al. 1997; van Leeuwen 2007), as well as precision optical BVI photometry, are available. We set $mag = I$, $M_{\text{abs}} = M_I$ and colors = $\{B-V, V-I\}$ in the set of parameters to be compared to the models. The models used for this comparison are from the PAdova TRieste Stellar Evolution Code (PARSEC, Bressan et al. 2012), with a narrow metallicity step of $[M/H] = 0.1$ and age steps of $\log \tau(\text{yrs}) = 0.05$.

Fig. 5 presents the comparison of our spectro-photometric distances (BPG) to those from Hipparcos, REF, taken as the reference sample. Each panel corresponds to a specific set of measured parameters \mathbf{x} , as listed in §2. The four alternative sets proposed in this paper provide distances that are in agreement with the astrometric distances. The Hipparcos sample is volume limited, as reflected by the upper boundary at $d \simeq 58$ pc for their distances. After a $3\text{-}\sigma$ clipping, the mean and dispersion of the relative distance residuals in the four panels, from (a) to (d), are $-5.0 \pm 19.8\%$, $-4.7 \pm 18.4\%$, $-5.7 \pm 18.2\%$, and $-2.4 \pm 17.6\%$. The negative average residual in all panels confirms the visual impression of a slight systematic effect of underestimating distances to these nearby stars. The results for the different parameter sets are quite similar, although the purely spectroscopic set (2) leads to a larger number of objects with distances determined, and a slightly lower scatter but stronger systematics for $d < 50$ pc. The figure confirms the results from our simulated stars that all four sets may be used to estimate reliable distances, provided that the photometric and spectroscopic parameters are accurate enough.

Fig. 6 shows the relative distance residuals taken from set (1) as a function of the main spectroscopic parameters for all reference samples used in this Section. The top row refers to the Hipparcos sample. There is little or no systematics in the residuals with the parameters themselves. The main trend observed is with T_{eff} , in the sense that the distances are systematically underestimated for the hotter stars. This may be caused by stellar rotation. Fast rotation may pose an issue to spectroscopically-determined stellar parameters. In fact, if we restrict our distance comparison to moderately cool stars ($T_{\text{eff}} < 5800$ K), the mean relative residual drops below 1% for all parameter sets, except for parameter set 4, for which it is 3%. The dispersion around the mean residual remains similar to those for the entire sample.

Even though the 4 sets of parameters seem to yield acceptable distances, in the subsequent validation analyses in this paper we will concentrate on parameter set 1, since it makes use of a more complete set of spectroscopic and photometric parameters and their errors that are common to the surveys to which we are applying our method.

3.2. APOGEE

APOGEE has acquired high-resolution Near Infra-red (NIR) spectra ($R \simeq 22,500$) of $> 100,000$ stars selected from the 2MASS Point Source Catalogue (Cutri et al. 2003), most of which are red giant stars located at low Galactic latitudes. APOGEE is providing a unique spectroscopic sample of disk-dominated stars with unprecedented volume and depth coverage, for which precision kinematical and abundance measure-

ments are available. For more on APOGEE data, we refer to Ahn et al. (2014); Alam et al. (2015), and Holtzman et al. 2015 (*in prep*). Validation of ASPCAP products partly relies on calibrating star clusters with many confirmed member stars with well-determined parameters (Mészáros et al. 2013). In this section we use two APOGEE subsamples to test our distances. In §3.2.1, we use a set of stars in common with the CoRoT LRA01 anticenter field (Miglio et al. 2013a), whose asteroseismology analysis has led to precision atmospheric parameters. In §3.2.2, we make use of the APOGEE cluster dataset (kindly provided by Sz. Mészáros).

For APOGEE, we set $m = K_s$, $M_{\text{abs}} = M_{K_s}$, and colors = $\{(J-H), (H-K_s)\}$, all of which are corrected for extinction before computing the distances. For the cluster stars, extinction values are based on the Rayleigh-Jeans Color Excess method (RJCE, Majewski et al. 2011; Nidever et al. 2012; Zsawski et al. 2013). This method is based on stellar colour excesses measured using fluxes in near and mid infra-red bands, where almost all stellar spectra are in the Rayleigh-Jeans regime and therefore have very similar intrinsic colours. For the stars in common with CoRoT, extinction corrections are based on the method described by Schultheis et al. (2014).

As described in detail in Anders et al. (2014), we adopt ASPCAP T_{eff} as derived, without the shift proposed by Mészáros et al. (2013) to bring them into agreement with the T_{eff} scale based on the infra-red flux method. The reason is that the ASPCAP values are in very good agreement with optical high-resolution studies over a wide parameter range.

ASPCAP metallicities are the same cluster calibrated values from Mészáros et al. (2013) and include values that quantify deviations of α element abundances from solar pattern, $[\alpha/M]$. Since $[\alpha/Fe]$ is again available, we also assume that $[M/H] = [Fe/H] + [\alpha/Fe]$ for APOGEE stars³

For the comparison with the CoRoT sample (§3.2.1), APOGEE surface gravities were replaced by those from asteroseismic relations (Miglio et al. 2013a). As for the clusters (§3.2.2), the ASPCAP $\log g$ values were also recalibrated based on asteroseismic data from CoRoT and Kepler (the APOKASC catalogue; Pinsonneault et al. 2014) missions, as described in Anders et al. (2014). Table 2 summarizes the data provenance.

3.2.1. APOGEE - comparison with asteroseismology: the CoRoT LRA01 field

One important test for our distance method is the comparison with asteroseismically derived distances. It has been shown by recent studies (e.g., Miglio 2012; Silva Aguirre et al. 2012, 2013) that stellar distances (or equivalently, radii) determined from CoRoT and Kepler lightcurves, either via asteroseismic scaling relations or by comparing asteroseismic parameters to predicted values from a grid of models, agree within a few percent with Hipparcos parallaxes and eclipsing binary data. For example, Silva Aguirre et al. (2012) show that distances can be derived with 5% precision for solar-like stars by coupling the infra-red flux method to determine T_{eff} and bolometric fluxes to the grid-modelling of the measured values of maximum power oscillation frequency and of frequency difference between dominant oscillation modes. We therefore compared our spectro-photometric distances based on set (1) of measured parameters with the dis-

³ We here refer to ASPCAP's cluster-calibrated $[M/H]$ values (Ahn et al. 2014; Mészáros et al. 2013) as $[Fe/H]$, as ASPCAP metallicities were calibrated on literature $[Fe/H]$ values.

Table 3. Summary of the results for the reference distance samples used in this work.

Sample	N_{stars}	Dist. Range (kpc)	Mean rel. residuals [%]	RMS rel. residuals [%]
Simulated stars	10000	= 3.16	0.9	18.5
HARPS-Hipparcos	372	< 0.060	-5.0	19.8
HARPS-Hipparcos ($T_{\text{eff}} < 5800$ K)	212	< 0.060	-0.2	21
CoRoT-APOGEE	118	1 – 6	-9.1	11.3
CoRoT-APOGEE	28	> 3	-13.9	18.5
APOGEE clusters – field priors	98	1 – 5	0.9	30.4
APOGEE clusters – cluster age prior	97	1 – 5	9.0	34.4
SEGUE clusters – field priors	410	1 – 12	15.8	44.1
SEGUE clusters – field priors	126	< 5	2.8	27.3
SEGUE clusters – $\Delta \log g = +0.25$ dex; field priors	418	1 – 12	-2.4	34.0
SEGUE clusters – $\Delta \log g = +0.25$ dex; field priors	130	< 5	-18.1	12.4
SEGUE clusters – $\Delta \log g = +0.25$ dex; clus. age priors	372	1 – 12	18.8	47.5
SEGUE clusters – $\Delta \log g = +0.25$ dex; clus. age priors	106	< 5	-16.4	17.8

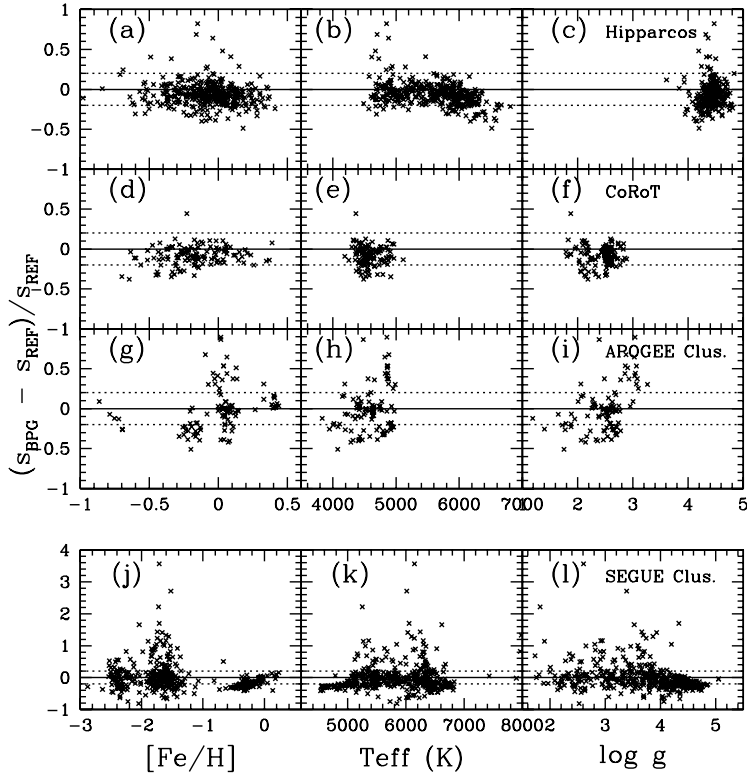


Fig. 6. Relative residuals in our distances (based on parameter set (1)) plotted as a function of the main spectroscopic parameters. Top row: Hipparcos sample; 2nd row: APOGEE/CoRoT; 3rd row: APOGEE clusters; bottom row: SEGUE clusters. Left panels (*a,d,g,j*): distance residuals as a function of $[\text{Fe}/\text{H}]$. The central dashed line is the identity line, whereas the upper and lower ones indicate deviations at the 20% level; Middle panels (*b,e,h,k*): distance residuals as a function of T_{eff} ; Right panels (*c,f,i,l*): residuals as a function of $\log g$.

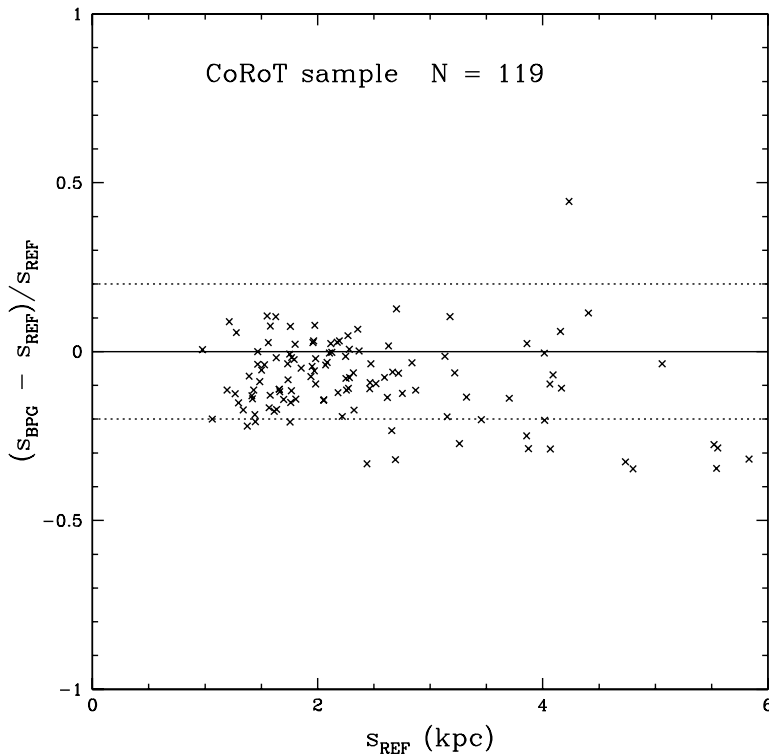


Fig. 7. Relative residuals between our spectro-photometric distances (using CoRoT $\log g$ and APOGEE T_{eff} , $[M/H]$ and $[\alpha/M]$) and the distances derived from asteroseismic modelling for 120 stars in the CoRoT LRA01 field. Only results based on the larger set of measured parameters (set (1) listed in §2) are shown. The number of stars contributing to the plot is given. The stars span a distance range from 1 to ~ 6 kpc. Dashed lines again represent the identity line and the 20% deviations from it.

tances obtained from CoRoT data for 120 stars in the anticenter field LRA01 which have been observed by both instruments.

The comparison is shown in Fig. 7. We again show the relative distances residuals between our distances (BPG) and those from CoRoT (REF). The general picture is reassuring, despite the low number statistics. The mean and rms residuals are -0.09 ± 0.12 . For distances > 3 kpc the systematic trend towards underestimating the distances increases to -0.14 ± 0.18 . Still, the concordance of both methods is remarkable. At the moment, we attribute most of the systematics to our method, but we cannot completely exclude that CoRoT distances are subject to small systematics (e.g., in the effective temperature scale) as well. We conclude that our method works relatively well and that only small systematic shifts in the scale are visible at least out to distances of ~ 5 kpc.

In the second row of Fig. 6 we show the relative distance residuals plotted as a function of the main spectroscopic param-

eters, similar to what was done for the Hipparcos sample. No strong trends are seen with metallicity, effective temperature or surface gravity.

3.2.2. APOGEE - Cluster comparison

In Fig. 8, we compare our spectro-photometric distances with those obtained from isochrone fitting of star cluster color-magnitude diagrams (CMDs). We again restrict the comparison to the spectro-photometric distances based on the parameter set (1) in §2. We use a subsample of the ~ 500 open and globular cluster stars that are used for calibration of ASPCAP, as described in Mészáros et al. (2013). We again refer to Table 2 for a summary of the data used. Most of the 104 stars with reliable parameters belong to the open clusters M 67, NGC 6791 and NGC 6819, but there are also some (≥ 5) members of the open clusters NGC 188, NGC 7789, NGC 2420, NGC 2158 and the old

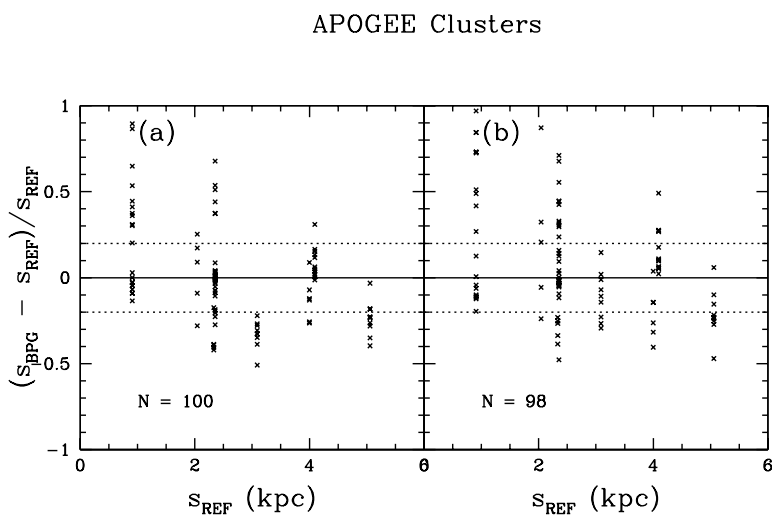


Fig. 8. Relative residuals between our APOGEE spectro-photometric distances and the distances obtained from cluster isochrone fitting. Panel (a): all priors as discussed in §2.1 are used; Panel (b): a simple prior on the age of each cluster is used. We also show the identity (solid) line and the 20% deviations from it (dashed lines).

globular cluster M 71. The cluster distances and ages are adopted from the WEBDA cluster database in the case of open clusters and Harris (1996) for the globular clusters. Table 4 summarizes the cluster properties.

The left panel on the figure shows the results for the priors discussed in §2.1, which are adequate for field stars. There is a hint for a small systematic trend in our distances towards being (under)overestimated for (more)less distant clusters. But the global mean residual is actually very small, of only 1%, although with a rms scatter of 30%. All clusters, except for NGC 2420 ($s_{\text{REF}} \approx 3$ kpc), have most of their stars with residuals smaller than 30%. The systematic trend with distance is improved by adoption of a simple age prior on each cluster, as shown in panel (b) of the same figure. This adopted *cluster prior* simply assumes a lognormal distribution of cluster stellar ages, whose mean is the best age estimate for the cluster and the dispersion is taken as $d \log \tau = 0.1$. This age prior improves the agreement with the reference distances for NGC 2420 and NGC 2158, but negatively

affects M71, which is the oldest and most metal poor cluster in the list.

The comparison suggests that our spectro-photometric method, despite the scatter, yields distances that are in good general agreement with the cluster scale. In the third row of Fig. 6 we again show the distance residuals as a function of metallicity, effective temperature and surface gravity. The points are grouped around specific values of these parameters, as expected for stars in clusters. The residuals also reflect the results from the previous figure. The large residuals for $[\text{Fe}/\text{H}]$ close to solar are due to stars in NGC 2420 and NGC 6819. Because they rank among the youngest systems in the APOGEE cluster list, these two clusters tend to contribute with relatively hotter and higher *logg* members to the APOGEE sample.

Regarding the uncertainty of isochrone-based cluster distances, it has been shown by Pinsonneault et al. (2000) that open cluster distances (which are usually determined via measuring the main-sequence shift relative to the Hyades cluster) may be

Table 4. Summary of the properties of star clusters used as reference for APOGEE distance estimates.

Cluster	$m - M$	$\log(\tau)$	[Fe/H]	E(B-V)
M 67	9.79	9.41	0.00	0.03
NGC 188	11.55	9.63	-0.02	0.08
NGC 2158	13.52	9.02	-0.23	0.66
NGC 2420	12.45	9.05	-0.26	0.04
NGC 6791	13.06	9.64	+0.15	0.14
NGC 6819	11.86	9.17	+0.07	0.18
NGC 7789	11.84	9.23	-0.08	0.36
M 71	13.01	10.00	-0.78	0.28

subject to zero-point shifts, based on changes in the adopted distance to the Hyades and interstellar reddening, as well as to the metal and helium abundance of the Hyades. However, assuming a conservative error of 0.1 mag for the cluster distance moduli, the uncertainties in the spectroscopic distances are still by far the most important.

3.3. SEGUE

The Sloan Extension for Galactic Understanding and Exploration (SEGUE) is a large optical spectroscopic survey at low resolution ($R \approx 2,000$, Smeed et al. 2013). Its goal is to deepen our knowledge about the Galactic structural components and their stellar content, sampling them mostly at high latitudes (Yanny et al. 2009; Eisenstein et al. 2011). In this sense, SEGUE is largely complementary to APOGEE in terms of coverage of the Galactic components. For more info on the spectra and instruments we refer to Gunn et al. (2006) and Smeed et al. (2013). SEGUE data have been processed through the SEGUE Stellar Parameter Pipeline (SSPP), which is described, along with its improvements, in a series of papers (Lee et al. 2008a,b; Allende Prieto et al. 2008b; Smolinski et al. 2011; Lee et al. 2011a). Particularly important to the SSPP is the validation of the derived stellar parameters. Field stars with high-resolution spectra and known members of well studied star clusters have been used for that purpose (Allende Prieto et al. 2008b; Lee et al. 2008b; Smolinski et al. 2011).

As in the case of APOGEE (see §3.2.2), we here use the sample of cluster stars, whose distances are well-known from isochrone fitting, to further test our distance estimates. In the case of SEGUE data, we set $\text{mag} = g$, $M_{\text{abs}} = M_g$, and colors = $\{(u - g), (g - r), (r - i), (i - z)\}$ (see Gunn et al. (1998) for a description of the SDSS camera and Fukugita et al. (1996) for information on the photometric system). The spectroscopic and photometric data are from the SDSS *Ninth Data Release* (DR9; Ahn et al. 2012) database. Since $[\alpha/\text{Fe}]$ is available for all SEGUE stars in our reference clusters, we assume that $[M/\text{H}] = [\text{Fe}/\text{H}] + [\alpha/\text{Fe}]$ in order to compare the data to the model $[M/\text{H}]$ values. As previously mentioned, all measured quantities have associated uncertainties. The measured photometric quantities also must be corrected for extinction and reddening to allow a direct comparison to the models. The clusters used here are listed in Table 5.

The original sample contained 11 clusters, among open and globular, totalling a bit over 1000 stars. For 593 stars, a complete set of spectroscopic and photometric parameters and associated uncertainties allowed us the use of parameter set (1) to estimate distances. As the sample is spectroscopic, in all other cases the missing parameter(s) was(were) photometric. Distances were successfully computed (i.e., at least one model was found within 3σ of all the measured quantities) for 425 out of the 593 stars, pertaining to the eight clusters listed in the table. We include only

those clusters with at least five confirmed members and successfully derived distances using our approach. Their distances, ages and metallicities were again taken from the WEBDA database in the case of open clusters, and from Harris (1996) in the case of the globular clusters.

Fig. 9 compares our spectro-photometric distances with the cluster distances for different $\log g$ calibrations and/or priors used to compute the distances. Panel (a) shows the relative distance residuals for the SEGUE cluster stars using the SEGUE data as they come from DR9. The mean and rms residuals are 0.16 ± 0.44 after applying a $3\text{-}\sigma$ clipping. In particular, our distances are biased towards large values for a significant fraction of the stars in the more distant globular clusters. If we consider only the 3 clusters with $s_{\text{REF}} < 5$ kpc, the mean and rms scatter are reduced to 0.03 ± 0.27 .

We investigated further the cause of this systematic overestimate of the distances to part of the SEGUE clusters. In analyzing the distribution of different SEGUE spectroscopic parameters, it became clear that the $\log g$ parameter for our sample, as published in DR9, appears to be underestimated for most stars in those clusters. Recalling that $\log g$ is the most important quantity to efficiently separate dwarf and giant stellar models, we have decided to heuristically correct for this shift in this work.

The contours (black) in Fig. 10 show the distribution of a large sample of SEGUE G-dwarf stars (sample compiled from DR9 and described and analysed in Brauer et al. 2015 (*in prep.*)) in the $\log g$ vs. T_{eff} (left panel) and $\log g$ vs. [Fe/H] (right panel) plane. For comparison, we also present the density distributions for a mock sample of G-dwarf stars obtained from TRILEGAL simulations (Girardi et al. 2005, 2012) covering the same SEGUE plates as present in the SEGUE G-dwarf data sample. These simulations were carried out using ADDSTAR, a web based tool that uses parallel processing to efficiently run TRILEGAL in many independent pointings (Balbinot et al. 2012). The TRILEGAL G-dwarf mock sample shown here has been compiled by applying the same overall cuts to the simulation that were used for the SEGUE G-dwarf data sample including the colour-magnitude limits for SEGUE G-dwarfs. For a detailed description of the TRILEGAL mock sample see Brauer et al. 2015 (*in prep.*).

A clear shift is seen in both panels, in the sense that the data have systematically lower values of $\log g$ for a fixed T_{eff} or metallicity by ≈ 0.25 dex. The comparison with the population synthesis model reveals that the SSPP $\log g$ values published in DR9 are underestimated, and that shifting the $\log g$ values for the SEGUE stars is clearly needed, at least for the purpose of deriving reliable distances. Further details about the TRILEGAL mock G-dwarf sample, the discrepancies seen in stellar parameters between data and simulation, and the underestimated surface gravity values published with DR9 are given in Brauer et al. 2015 (*in prep.*).

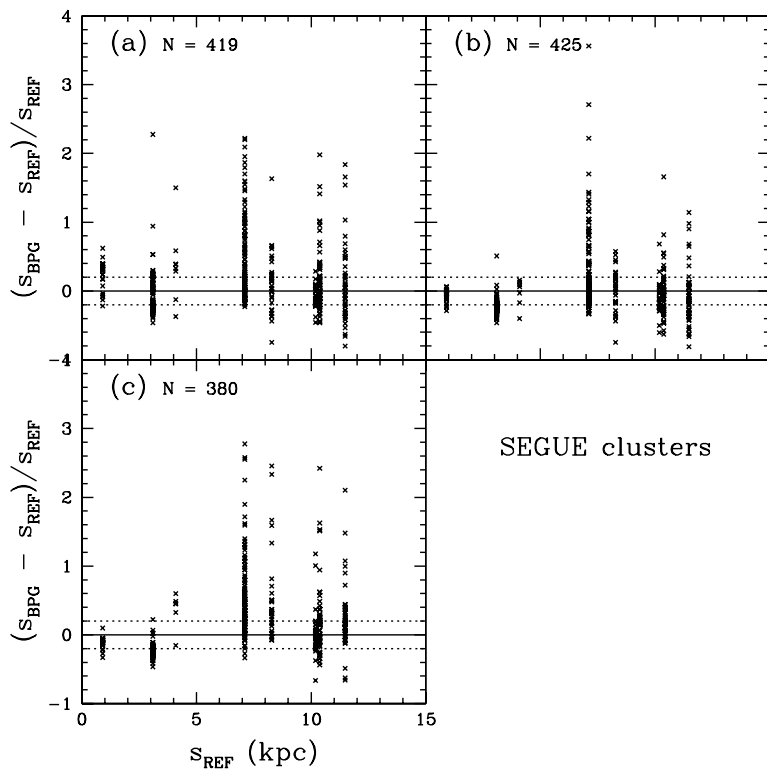


Fig. 9. Relative differences between our SEGUE spectro-photometric distances and those obtained from cluster isochrones. Panel (a): “uncorrected” SEGUE/SSPP parameters and field priors (see §2); Panel (b): a $\log g$ shift of $+0.25$ dex was applied to compatibilize the SEGUE $\log g$ scale with the expected values from stellar evolutionary models; Panel (c): shifted $\log g$ plus a simple prior on the cluster age instead of using the Galactic field priors.

Table 5. Summary of the properties of star clusters used as reference for SEGUE distance estimates.

Cluster	$m - M$	$\log(\tau)$	[Fe/H]	E(B-V)
NGC2420	12.45	9.05	-0.26	0.04
NGC6791	13.06	9.64	+0.15	0.14
M67	9.79	9.41	0.00	0.03
M2	15.30	> 10	-1.65	0.04
M3	15.04	> 10	-1.50	0.01
M13	14.26	> 10	-1.53	0.01
M15	15.08	> 10	-2.37	0.10
M92	14.59	> 10	-2.31	0.02

We thus decided to test the effect of applying a shift of 0.25 dex to the $\log g$ values when computing the distances. The results are shown in panel (b) of Fig. 9. The global mean offset relative to the reference distances has been reduced to -2.4% , although the rms relative residual remains high (34%). For the three more nearby clusters, the distances are now systematically

underestimated by -18% although the scatter around the mean residual has decreased considerably to 12%. The result of adopting a simple age prior for the clusters, as done for APOGEE data, is shown on panel (c) of Fig. 9. This choice has a sizable effect on the distances in the sense of increasing the distances for the more distant clusters, yielding a mean and rms relative residual

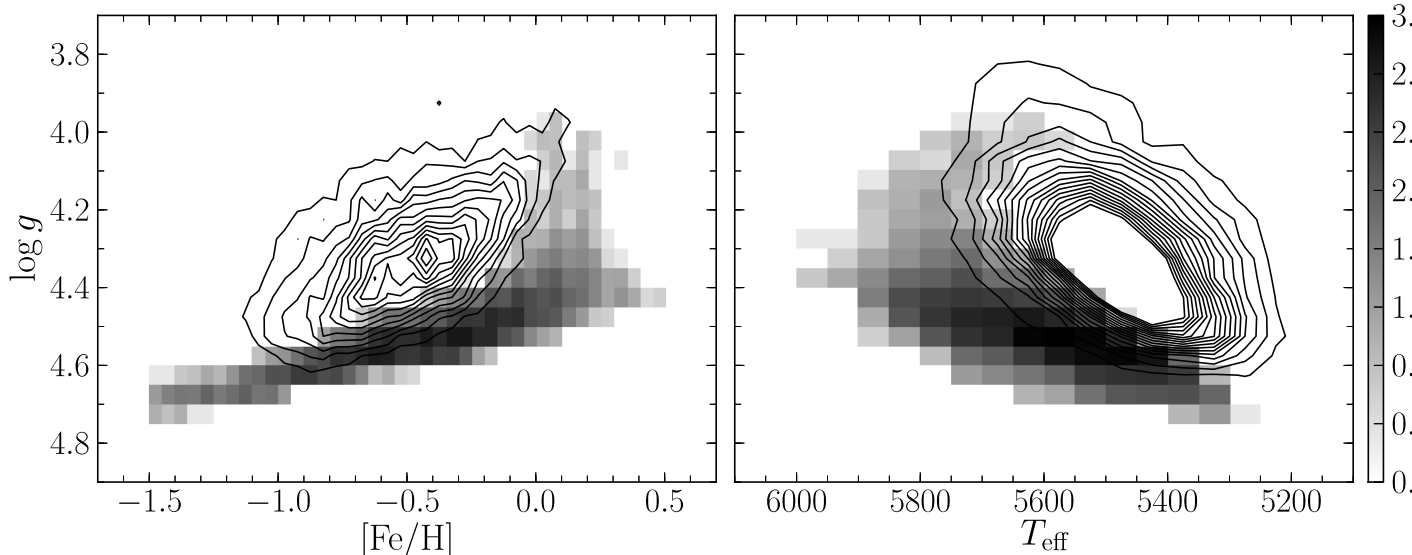


Fig. 10. Left panel: The contours show the density of SEGUE dwarfs in the $\log g$ vs. $[\text{Fe}/\text{H}]$ plane. The colour density map corresponds to the same type of stars simulated by the Trilegal code. Right panel: same as in the previous panel, but stars are shown in the $\log g$ vs. T_{eff} plane.

of 0.19 ± 0.47 . Notice that this trend goes in the same direction as in the case of APOGEE (see §3.2.2).

We conclude that there is a general agreement between our distances for SEGUE stars and those from CMD fitting. This is certainly true for the three clusters with reference distances less than 5 kpc, regardless of any *ad hoc* rescaling of the $\log g$ values from DR9. The main problem with SEGUE, therefore, resides with the more distant clusters, whose distances are significantly overestimated by our code, specially if the DR9 $\log g$ data are used with no recalibration.

In the last row of Fig. 6 we show the distance residuals against $[\text{Fe}/\text{H}]$, T_{eff} , and $\log g$, similarly to what we did with the other samples used as reference. The figure clearly shows that most of the stars have residuals close to or within the 20% lines and do not exhibit any strong systematics with these parameters. The more deviant points are restricted to a fraction of the low metallicity ($[\text{Fe}/\text{H}] < -1.5$) giant ($\log g \leq 3$) stars which dominate the SEGUE sample in the globular clusters.

Finally, we emphasize that the SEGUE data is very distinct from APOGEE in terms of spectral range and resolution. It also probes much larger distances than the Hipparcos based data used in §3.1.

3.4. RAVE

RAVE collected medium-resolution ($R \sim 7,500$) CaII triplet spectra of $\geq 400,000$ stars with $9 < I < 13$. For $> 200,000$ of these stars, Burnett et al. (2011) have been able to derive spectro-photometric distances using spectroscopic parameters from the RAVE pipeline (Kordopatis et al. 2011) as well as near infrared photometry from 2MASS (Skrutskie et al. 2006; Cutri et al. 2003). Their method has provided the background for the work presented in this paper, which is largely based on the Bayesian approach proposed by Burnett et al. (2011). More recently, Binney et al. (2014) presented an improved version of the method. In this section, we use their distances for a high S/N sample containing ≥ 8000 giant stars (Boeche et al. 2013) to cross-check

the implementation of our method. The spectroscopic parameters are taken from the RAVE Data Release 4 (DR4; Kordopatis et al. 2013), whereas the photometry is from 2MASS.

In order to derive distances for RAVE stars, we set $m = K_s$, $M_{\text{abs}} = M_{K_s}$, and colors = $\{(J - H), (H - K)\}$. We adopt the A_V extinction values that have been computed for individual RAVE objects by Binney et al. (2014) to deredden the NIR magnitudes of the stars. The conversion between the extinction in the optical and near-IR wavelength range is performed following Rieke & Lebofsky (1985). We adopted the $[\alpha/\text{Fe}]$ estimates from the chemical RAVE pipeline (Kordopatis et al. 2013) to make our metallicity scale more compatible with the stellar models, as in the previous sections.

Fig. 11 shows the comparison of our distance estimates with the distances from Binney et al. (2014) for the giant sample analyzed in Boeche et al. (2013). For compatibility with our approach described in §2, we use the $\langle s \rangle$ distance estimate from Binney et al. (2014) in this comparison, which is the expectation value computed from their model pdf over distances instead of their corresponding parallaxes. Because neither of the distances being compared are supposed to be at the same level of precision as those that we consider as reference samples, we change the way we compare them. Instead of computing the relative residual with respect to any one of the estimates, we normalize the residual by the combined uncertainty from both, which are added in quadrature. Our distance scale seems to be slightly compressed relative to RAVE DR4: we have systematically larger (smaller) distances than RAVE for stars with $s_{\text{RAVEDR4}} < 1$ ($s_{\text{RAVEDR4}} > 1$) kpc. The effect, however, is small. The vast majority of the stars have distance residuals well accommodated by the expected uncertainties in the two estimates being compared. The mean and rms normalized residuals are 0.00 ± 0.33 , after a $3\text{-}\sigma$ clipping to eliminate the very few strongly deviant points between the two methods. Looking separately at the two distances regimes, we have mean relative residuals of 6% and -16%, respectively for $s_{\text{RAVEDR4}} < 1$ and $s_{\text{RAVEDR4}} > 1$ kpc.

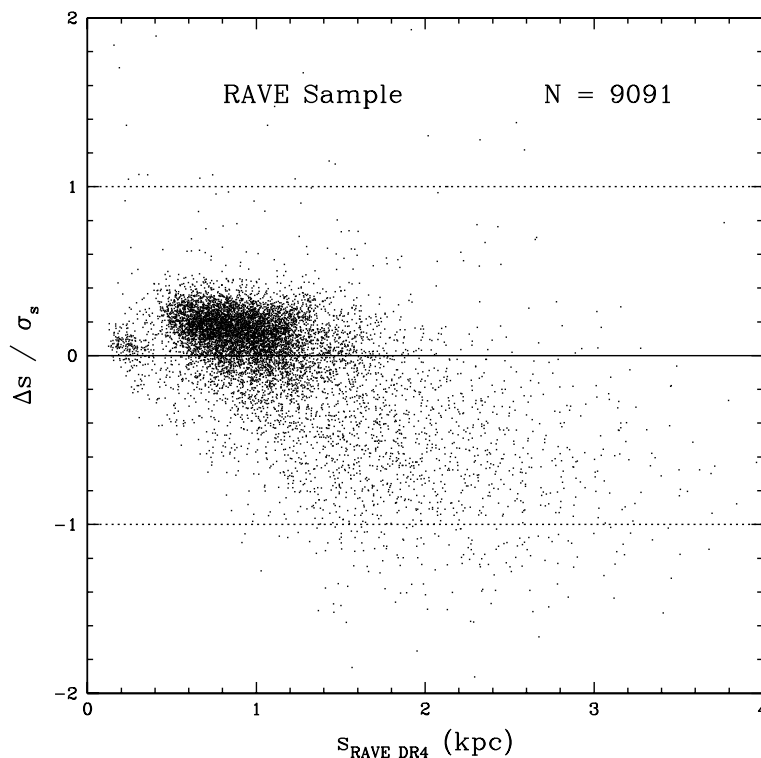


Fig. 11. Difference between distances from this work and those from Binney et al. (2014) plotted against those from Binney et al. (2014) for a set ≈ 9000 giant stars with high S/N obtained as part of the RAVE collaboration. The distance differences are normalized by their combined uncertainties. Distances from Binney et al. (2014) are the expectation values taken directly from the distance distribution functions.

4. Summary and conclusions

We have implemented a code to estimate distances to field stars based on their measured spectroscopic and photometric parameters. The theoretical background is essentially the same as that of Burnett & Binney (2010) and subsequent papers from the same authors. Briefly, given a set of measured quantities, these are compared to model values and, using a Bayesian approach, the posterior probability distribution function is derived for each star. The distance is then determined by a weighted average over this pdf.

We used simulated stars from PARSEC models as a first validation test of our distances. We showed that distances based on 4 different sets of parameters are well recovered, without systematics. The method starts breaking down if $\log g$ is removed from the data set, yielding unacceptably large errors. Not surprisingly, the errors in the estimated distances increase with the uncertain-

ties in the measured parameters used in the method. A larger set of such parameters also tends to lead to smaller distance errors.

We have computed distance uncertainties in three different ways for all stars, and intercompared them. We conclude that, for most stars, the largest source of uncertainty arises from the model pdf width, meaning that a large variety of stellar types (with variable luminosities) can still account for the set measured quantities; however, distances may also vary significantly for a given star by simply changing the data set to be compared to the models. For a large sample of SEGUE G dwarfs, for instance, the estimated uncertainties tend to be larger when a distance based only on spectroscopic parameters is computed (see Fig. 4).

We demonstrated that distances of nearby stars with parallaxes from Hipparcos and precise atmospheric parameters are successfully recovered, with small systematic trends. The relative random errors are of the order of 20% or less.

For more distant stars, we have validated the code using well-studied star clusters by inferring distances for many of their certain members and comparing them to the cluster distances taken as reference in the literature. We used star clusters included in the SDSS-III SEGUE and APOGEE samples for that purpose. In the case of SEGUE data, there are no strong systematics in the estimated distances for the three clusters closer than ≈ 6 kpc. Beyond that our distances tend to be overestimated by more than 30%. Part of the effect is caused by the SSPP $\log g$ scale, which appears to be too low by ≈ 0.25 dex for main-sequence and sub-giant branch stars when compared to stellar evolutionary models of similar metallicity and T_{eff} . The lower surface gravities tend to make the stars overluminous, since they are more frequently matched to subgiant and giant models. Correcting for this effect reduces the systematics at larger distances to 15%. The rms error for SEGUE is higher than for the Hipparcos sample, of the order of 35%. But Fig. 6 shows that most stars have residuals relative to the reference host cluster distances of $\leq 20\%$.

In the case of APOGEE, no *ad hoc* correction to the atmospheric parameters had to be applied to bring the estimated distances into reasonable agreement with those of the clusters. This may be due to the higher spectral resolution, coupled with the fact that APOGEE $\log g$ values could be anchored to more precise estimates from asteroseismology. Only a slight systematic trend is seen in our distances compared to those from the literature, while the random scatter is similar to that seen in the SEGUE sample after the recalibration of the $\log g$.

We tested our distances against those derived from asteroseismic observations. The sample consists of ≈ 120 stars in common between APOGEE and CoRoT samples. The CoRoT parameters and distances were derived independently from APOGEE. There is a general agreement between our distances and those from the CoRoT collaboration, with a scatter of $\approx 15\%$, although with a systematic offset (our distances are systematically smaller) of $\approx 10\%$.

We have also compared our distances to those from authors who have used similar approaches. Despite the large scatter and a slight systematic trend, our distances for a sample of red giant stars studied in Boeche et al. (2013) agree, within the expected uncertainties, with those derived by Binney et al. (2014) for the same stars.

The validation results are all summarized in Table 3, where we show the dataset used, the number of stars and the range of reference distances in each, and the mean and rms relative residuals. The table allows a global evaluation of the distances, specially when confronted to those from astrometry, asteroseismology, and well calibrated star clusters. The systematic residuals are usually less than 9% while the scatter scales with the quality of the input spectro-photometric parameters, with the most distant SEGUE clusters being our worst case.

The code presented and validated in this paper is being used by the Brazilian Participation Group on SDSS-III to derive distances for tens of thousands of stars belonging to the SEGUE and APOGEE surveys. These surveys are complementary in many ways, including the directions and Galactic components they probe more efficiently. When analyzed together, provided that reliable distances are available, they allow a 3D mapping of Galactic structure using different stellar tracers, determination of chemo-kinematic relations in the Galaxy, and ultimately, confrontation of these constraints with models of Galactic formation and evolution (Minchev et al. 2013, 2014). Initial science analyses based on these distances are provided by Brauer et al 2015 (*in prep.*) and Anders et al. (2014).

Acknowledgements. Funding for SDSS-III has been provided by the Alfred P. Sloan Foundation, the Participating Institutions, the National Science Foundation, and the U.S. Department of Energy. The SDSS-III web site is <http://www.sdss3.org/>. SDSS-III is managed by the Astrophysical Research Consortium for the Participating Institutions of the SDSS-III Collaboration including the University of Arizona, the Brazilian Participation Group, Brookhaven National Laboratory, University of Cambridge, University of Florida, the French Participation Group, the German Participation Group, the Instituto de Astrofísica de Canarias, the Michigan State/Notre Dame/JINA Participation Group, Johns Hopkins University, Lawrence Berkeley National Laboratory, Max Planck Institute for Astrophysics, New Mexico State University, New York University, the Ohio State University, University of Portsmouth, Princeton University, University of Tokyo, the University of Utah, Vanderbilt University, University of Virginia, University of Washington, and Yale University. Funding for the Brazilian Participation Group has been provided by the Ministério de Ciência e Tecnologia (MCT), Fundação Carlos Chagas Filho de Amparo à Pesquisa do Estado do Rio de Janeiro (FAPERJ), Conselho Nacional de Desenvolvimento Científico e Tecnológico (CNPq), and Financiadora de Estudos e Projetos (FINEP). TCB acknowledges partial support for this work from grant PHY 08-22648: Physics Frontier Center / Joint Institute for Nuclear Astrophysics (JINA), awarded by the US National Science Foundation. This research has made use of the WEBDA database, operated at the Institute for Astronomy of the University of Vienna

References

- Ahn, C. P., Alexandroff, R., Allende Prieto, C., et al. 2014, *ApJS*, 211, 17
 Ahn, C. P., Alexandroff, R., Allende Prieto, C., et al. 2012, *ApJS*, 203, 21
 Alam, S., Albareti, F. D., Allende Prieto, C., et al. 2015, *ArXiv e-prints*
 Allende Prieto, C., Majewski, S. R., Schiavon, R., et al. 2008a, *Astronomische Nachrichten*, 329, 1018
 Allende Prieto, C., Sivarani, T., Beers, T. C., et al. 2008b, *AJ*, 136, 2070
 Anders, F., Chiappini, C., Santiago, B. S., et al. 2014, *A&A*, 564, 115
 Bailer-Jones, C. A. L. 2011, *MNRAS*, 411, 435
 Balbinot, E., Santiago, B., Girardi, L., et al. 2012, in *Astronomical Society of the Pacific Conference Series*, Vol. 461, *Astronomical Data Analysis Software and Systems XXI*, ed. P. Ballester, D. Egret, & N. P. F. Lorente, 287
 Binney, J., Burnett, B., Kordopatis, G., et al. 2014, *MNRAS*, 437, 351
 Boeche, C., Chiappini, C., Minchev, I., et al. 2013, *A&A*, 553, A19
 Bovy, J., Allende Prieto, C., Beers, T. C., et al. 2012a, *ApJ*, 759, 131
 Bovy, J., Rix, H.-W., Liu, C., et al. 2012b, *ApJ*, 753, 148
 Breddels, M. A., Smith, M. C., Helmi, A., et al. 2010, *A&A*, 511, A90
 Bressan, A., Marigo, P., Girardi, L., et al. 2012, *MNRAS*, 427, 127
 Burnett, B. & Binney, J. 2010, *MNRAS*, 407, 339
 Burnett, B., Binney, J., Sharma, S., et al. 2011, *A&A*, 532, A113
 Carollo, D., Beers, T. C., Bovy, J., et al. 2012, *ApJ*, 744, 195
 Carollo, D., Beers, T. C., Chiba, M., et al. 2010, *ApJ*, 712, 692
 Chabrier, G. 2003, *PASP*, 115, 763
 Cheng, J. Y., Rockosi, C. M., Morrison, H. L., et al. 2012, *ApJ*, 746, 149
 Correnti, M., Bellazzini, M., Ibata, R. A., Ferraro, F. R., & Varghese, A. 2010, *ApJ*, 721, 329
 Cutri, R. M., Skrutskie, M. F., van Dyk, S., et al. 2003, *2MASS All Sky Catalog of point sources*.
 Deng, L.-C., Newberg, H. J., Liu, C., et al. 2012, *Research in Astronomy and Astrophysics*, 12, 735
 Eisenstein, D. J., Weinberg, D. H., Agol, E., et al. 2011, *AJ*, 142, 72
 ESA, ed. 1997, *ESA Special Publication*, Vol. 1200, *THE HIPPARCOS and TYCHO catalogues. Astrometric and photometric star catalogues derived from the ESA HIPPARCOS Space Astrometry Mission*
 Fukugita, M., Ichikawa, T., Gunn, J. E., et al. 1996, *AJ*, 111, 1748
 Gilmore, G., Randich, S., Asplund, M., et al. 2012, *The Messenger*, 147, 25
 Girardi, L., Barbieri, M., Groenewegen, M. A. T., et al. 2012, *TRILEGAL, a TRIdimensional modeL of the GALaxy: Status and Future*, ed. A. Miglio, J. Montalbán, & A. Noels, 165
 Girardi, L., Groenewegen, M. A. T., Hatziminaoglou, E., & da Costa, L. 2005, *A&A*, 436, 895
 Gunn, J. E., Carr, M., Rockosi, C., et al. 1998, *AJ*, 116, 3040
 Gunn, J. E., Siegmund, W. A., Mannery, E. J., et al. 2006, *AJ*, 131, 2332
 Harris, W. E. 1996, *VizieR Online Data Catalog*, 7195, 0
 Hayden, M. R., Holtzman, J., Bovy, J., et al. 2014, *ApJ*
 Jørgensen, B. R. & Lindegren, L. 2005, *A&A*, 436, 127
 Jurić, M., Ivezić, Ž., Brooks, A., et al. 2008, *ApJ*, 673, 864
 Kordopatis, G., Gilmore, G., Steinmetz, M., et al. 2013, *AJ*, 146, 134
 Kordopatis, G., Recio-Blanco, A., de Laverny, P., et al. 2011, *A&A*, 535, A106
 Lee, Y. S., Beers, T. C., Allende Prieto, C., et al. 2011a, *AJ*, 141, 90
 Lee, Y. S., Beers, T. C., An, D., et al. 2011b, *ApJ*, 738, 187
 Lee, Y. S., Beers, T. C., Sivarani, T., et al. 2008a, *AJ*, 136, 2022
 Lee, Y. S., Beers, T. C., Sivarani, T., et al. 2008b, *AJ*, 136, 2050
 Majewski, S. R., Zasowski, G., & Nidever, D. L. 2011, *ApJ*, 739, 25

- Mészáros, S., Holtzman, J., García Pérez, A. E., et al. 2013, *AJ*, 146, 133
- Miglio, A. 2012, Asteroseismology of Red Giants as a Tool for Studying Stellar Populations: First Steps, ed. A. Miglio, J. Montalbán, & A. Noels, 11
- Miglio, A., Chiappini, C., Morel, T., et al. 2013a, in *European Physical Journal Web of Conferences*, Vol. 43, *European Physical Journal Web of Conferences*, 3004
- Miglio, A., Chiappini, C., Morel, T., et al. 2013b, *MNRAS*, 429, 423
- Minchev, I., Chiappini, C., & Martig, M. 2013, *A&A*, 558, A9
- Minchev, I., Chiappini, C., & Martig, M. 2014, *ArXiv e-prints*
- Minniti, D., Saito, R. K., Alonso-García, J., Lucas, P. W., & Hempel, M. 2011, *ApJ*, 733, L43
- Nidever, D. L., Zasowski, G., & Majewski, S. R. 2012, *ApJS*, 201, 35
- Perryman, M. A. C., de Boer, K. S., Gilmore, G., et al. 2001, *A&A*, 369, 339
- Perryman, M. A. C., Lindegren, L., Kovalevsky, J., et al. 1997, *A&A*, 323, L49
- Pinsonneault, M. H., Elsworth, Y., Epstein, C., et al. 2014, *ApJS*, 215, 19
- Pinsonneault, M. H., Terndrup, D. M., & Yuan, Y. 2000, in *Astronomical Society of the Pacific Conference Series*, Vol. 198, *Stellar Clusters and Associations: Convection, Rotation, and Dynamos*, ed. R. Pallavicini, G. Micela, & S. Sciortino, 95
- Pont, F. & Eyer, L. 2004, *MNRAS*, 351, 487
- Rieke, G. H. & Lebofsky, M. J. 1985, *ApJ*, 288, 618
- Rodrigues, T. S., Girardi, L., Miglio, A., et al. 2014, *MNRAS*, 445, 2758
- Schlesinger, K. J., Johnson, J. A., Rockosi, C. M., et al. 2012, *ApJ*, 761, 160
- Schönrich, R. & Bergemann, M. 2014, *MNRAS*, 443, 698
- Schultheis, M., Zasowski, G., Allende Prieto, C., et al. 2014, *AJ*, 148, 24
- Serenelli, A. M., Bergemann, M., Ruchti, G., & Casagrande, L. 2013, *MNRAS*, 429, 3645
- Silva Aguirre, V., Casagrande, L., Basu, S., et al. 2013, *Astronomische Nachrichten*, 334, 22
- Silva Aguirre, V., Casagrande, L., Basu, S., et al. 2012, *ApJ*, 757, 99
- Skrutskie, M. F., Cutri, R. M., Stiening, R., et al. 2006, *AJ*, 131, 1163
- Smee, S. A., Gunn, J. E., Uomoto, A., et al. 2013, *AJ*, 146, 32
- Smolinski, J. P., Lee, Y. S., Beers, T. C., et al. 2011, *AJ*, 141, 89
- Sousa, S. G., Santos, N. C., Israelian, G., Mayor, M., & Udry, S. 2011, *A&A*, 533, A141
- Steinmetz, M., Zwitter, T., Siebert, A., et al. 2006, *AJ*, 132, 1645
- van Leeuwen, F., ed. 2007, *Astrophysics and Space Science Library*, Vol. 350, *Hipparcos, the New Reduction of the Raw Data*
- Yanny, B., Rockosi, C., Newberg, H. J., et al. 2009, *AJ*, 137, 4377
- Zasowski, G., Johnson, J. A., Frinchaboy, P. M., et al. 2013, *AJ*, 146, 81
- Zwitter, T., Matijević, G., Breddels, M. A., et al. 2010, *A&A*, 522, A54